
Geometry-Induced Diffusion on Graphs: A Learnable Weighted Laplacian for Spectral GNNs

Mia Zosso^{*1} Ali Hariri^{*1} Victor Kawasaki-Borruat^{*1*} Pierre-Gabriel Berlureau^{*2}

Pierre Vandergheynst¹

¹École Polytechnique Fédérale de Lausanne (EPFL), Lausanne, Switzerland

²École Normale Supérieure – PSL, Paris, France

Abstract

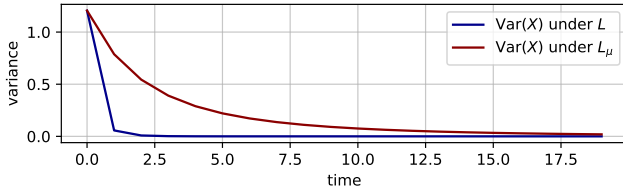
Long-range graph tasks are challenging for Graph Neural Networks (GNNs): global mechanisms such as attention or rewiring schemes can be computationally expensive, while deep local propagation is prone to vanishing gradients, oversmoothing, and oversquashing. The introduced μ -ChebNet architecture is a simple spectral GNN that learns a node-wise weight function μ before applying ChebNet-style filters. The learned weighting μ induces a modified graph Laplacian which effectively changes the propagation geometry without altering the graph topology. This task-dependent geometry promotes preferred routes for information propagation, thereby helping long-range signals avoid highly contractive bottlenecks, and obviating the need for repeated layer stacking. In practice, we replace the fixed graph Laplacian L by a learned operator L_μ , keeping the proposed μ -ChebNet architecture lightweight while making propagation task-adaptive. Furthermore, we provide a spectral analysis demonstrating how μ modulates propagation dynamics, and empirically observe improved performance on both synthetic long-range reasoning tasks and real-world graph benchmarks. The learned weight function is not only interpretable, but also offers a lightweight alternative to attention and rewiring for adaptive graph propagation.

1 Introduction

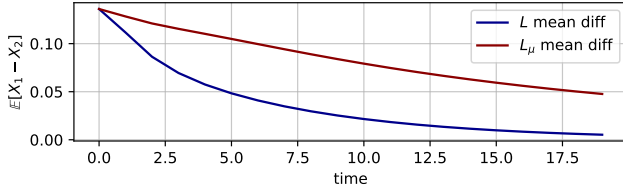
Graph Neural Networks (GNNs) [34, 7, 13] have achieved significant success in recent years, driving the development of novel architectures and investigations into their theoretical foundations. Alongside these advances, important limitations have also come to light, most notably oversmoothing and oversquashing [35, 33, 24, 3]. Oversmoothing makes node representations increasingly indistinguishable, while oversquashing compresses information from many distant nodes into limited-size embeddings. These effects are particularly damaging for long-range tasks, where relevant signals and gradients must cross many propagation steps and may progressively weaken [2].

Recent work has interpreted GNN layers through the lens of continuous dynamics, viewing propagation as the discretization of an evolution equation on the graph [31]. This view has motivated diffusion-based formulations that recast message passing as the discretization of partial differential equations (PDEs) on graphs, enabling principled control over information propagation through learnable diffusivity [8] or global attention mechanisms [40, 42]. Although the continuous GNN diffusion perspective provides a principled foundation for designing expressive architectures, it often leads to high computational complexity due to discretization.

^{*}Correspondence: victor.borruat@epfl.ch



(a) Variance of the signal along heat diffusion driven by L and L_μ .



(b) Difference in the mean of the signal between the SBM's two communities along heat diffusion driven by L and L_μ .

Figure 1: Filtering via heat diffusion using L (blue) and L_μ (red) on the Stochastic Block Model, where μ has a sharp variation at the community interface. The initial signal is white Gaussian noise. We observe slower variance contraction (a) under L_μ , indicating successful oversmoothing mitigation, as well as slower decay of the mean (b) between the signal on different communities X_1 and X_2 , respectively. This simple reweighting of the graph Laplacian significantly changes the information loss.

Another line of work addresses long-range propagation by dynamically rewiring the graph, for example by adding task-dependent edges or modifying the connectivity structure [20, 5]. While effective, such methods can introduce additional preprocessing cost, alter the original edge set and they may change the semantics of the input graph.

Conversely, spectral GNNs [13, 25] offer simple and computationally efficient architectures by leveraging the Fourier domain of the graph, only requiring to learn the fixed spectral filters' weights. Recent work on stabilization of the information flow across layers [18, 22] has shown that stabilized spectral GNNs can outperform most other GNNs on long-range tasks, and it is believed that they possess competitive generalization qualities [27]. Such spectral GNNs, however, still rely on a *fixed* graph Laplacian L , limiting their ability to adapt information flow to task-specific structure. In particular, *they lack a mechanism for locally steering information propagation*.

In this work, we introduce a task-adaptive graph Laplacian for spectral GNNs, producing a rewiring-like effect without actually rewiring the graph. Our key idea is to learn a node-wise density μ that determines where information flows more easily on the graph. Instead of propagating with the fixed Laplacian L , we construct a weighted Laplacian L_μ by reweighting each existing edge according to the learned densities at its endpoints. This is analogous to diffusion in an inhomogeneous medium, where spatial variations in the medium locally guide propagation. The induced dynamics acquire a learned propagation bias without introducing an explicit vector field, thus mitigating traffic through contractive bottlenecks and breaking spectral degeneracies, all while leaving the graph topology unchanged (Figure 1). We learn μ upstream and use the induced operator L_μ in place of the fixed Laplacian inside ChebNet-style spectral filters. This yields μ -ChebNet and μ -Stable-ChebNet, which combine task-adaptive propagation with efficient polynomial filtering. Rather than learning separate node-to-node communication weights as in attention, our method learns one density value per node. This induces edge weights on the fixed graph and biases transport toward task-relevant regions while keeping the model lightweight.

Our work makes the following contributions:

1. **A task-adaptive Laplacian for spectral GNNs.** We derive a discrete Laplacian L_μ whose entries depend on a learnable node-wise density μ . This replaces the fixed graph Laplacian with a learned propagation operator that preserves the original topology.
2. **Spectral control of propagation dynamics.** We characterize how the learned density μ reshapes the spectrum of L_μ . Under a fixed normalization of μ , this corresponds to redistributing spectral energy across modes. This changes the relative timing with which graph Fourier components are smoothed, providing a mechanism for delaying overmixing and modulating bottleneck-sensitive propagation.
3. **A new family of spectral GNNs.** We introduce μ -ChebNet and μ -Stable-ChebNet, two architectures that jointly learn (i) propagation dynamics through the density μ and (ii) spectral filters through Chebyshev polynomials. These models bridge spectral and message-passing viewpoints: they retain the efficiency of polynomial spectral filtering, while propagation

remains a local diffusion process along existing edges, now governed by a learned task-adaptive Laplacian rather than the fixed graph Laplacian.

4. **Extensive empirical evidence and interpretability.** Across synthetic long-range reasoning tasks and real-world benchmarks, our models are competitive with strong spectral baselines, with the most consistent gains obtained when the learned Laplacian is combined with stability constraints. The learned node-wise density μ also provides an interpretable graph signal, revealing where propagation is strengthened or attenuated for a given task.

Outline Section 3 reviews background on graph Laplacians, diffusive dynamics, and Chebyshev spectral filters. Section 4 introduces the weighted Laplacian on graphs, analyzes its spectral properties, and shows how it enhances standard spectral GNNs, leading to our μ -ChebNet architecture whose results we present in Section 5. The latter benchmarks our model on synthetic and real-world tasks. We conclude by illustrating how the learned weight function provides a simple and interpretable mechanism for task-dependent routing.

2 Related Work

Mitigating Oversmoothing & Oversquashing. Recent works propose PDE-inspired propagation dynamics, with an emphasis on controlling information flow through diffusion and transport mechanisms. GRAND casts GNN layers as discretizations of diffusion equations on graphs, where the choice of diffusivity and numerical scheme shapes propagation [9]. In Wu et al. [43], this view is extended through advective diffusion: global attention is interpreted as a non-local diffusion mechanism that captures latent interactions, while local message passing acts as an advection-like term that keeps the dynamics tied to the observed graph topology. While expressive and theoretically motivated, such approaches typically rely on attention-based coupling or the solution of continuous-time dynamics, which can introduce substantial computational overhead. Graph Transformers (GTs) [32] pursue a related goal from an architectural perspective, combining local aggregation with global attention to improve long-range communication. However, standard global attention scales quadratically in the number of nodes, motivating sparse GTs [36, 37, 10] and dynamical graph-rewiring schemes [1].

Efficient Spectral GNNs. Spectral GNNs (such as ChebNets [13]) have undergone a recent revival in relevance for both their computational efficiency and ability to capture long-range interactions via constructive graph Laplacian-based filters when stabilized [18]. These models are simple to implement and analyze due to the rich tools of spectral graph theory [11], and were also shown to consistently outperform MPNNs, graph rewiring techniques, and GTs on several long-range tasks [22].

Modified Graph Laplacians. Rather than designing new architectures, there has been considerable research done in finding different graph Laplacians, with hopes of enriching information propagation across the graph. Modern approaches include degree-dependent penalties [17], attractive & repulsive effects modeling [28], complex phases for orientation [45, 15], or control over spectral scaling [30]. All the aforementioned approaches remain constrained by the given graph structure and use propagation operators that are *fixed* independently of the task. In contrast, our adaptive Laplacian L_μ introduces a learnable node-wise weight function μ , yielding spatially varying, task-dependent transport while preserving the original graph topology. Rather than shortening paths by adding edges, this changes the effective transport geometry on the existing graph, creating preferred diffusion routes that can reduce the amount of repeated mixing required for long-range communication.

3 Background

In this section we recall elements of calculus on graphs, which will allow us to formulate drift-diffusion dynamics on graphs and derive both the classic notion of a graph Laplacian L , as well as the task-adaptive weighted Laplacian L_μ . We will also briefly recall the ChebNet architecture, as well as motivate this specific choice for the architecture we will subsequently introduce.

3.1 Calculus on Graphs

Let $\mathcal{G} = (V, E)$ be an undirected graph with $|V| = n$ vertices and $|E| = m$ edges. We denote by \mathcal{H}_V the Hilbert space of square-integrable *node signals* $f : V \rightarrow \mathbb{R}$, with corresponding scalar product $\langle f, g \rangle := \sum_{i=1}^n f(i)g(i)$, for i running over the nodes in V . Likewise, \mathcal{H}_E will denote the Hilbert space of square-integrable *edge signals* $G : E \rightarrow \mathbb{R}$. To define signed edge differences, we fix an arbitrary orientation of each undirected edge. This orientation is only a bookkeeping device and does not affect the Laplacian obtained below. The corresponding scalar product is given by $\langle\langle F, G \rangle\rangle := \sum_{e=1}^m F(e)G(e)$, for e running over the edges in E . We will reserve the use of capital letters for such edge signals.

For an oriented edge $e = (i, j)$, the *gradient operator on \mathcal{G}* is denoted $\nabla^{\mathcal{G}} : \mathcal{H}_V \rightarrow \mathcal{H}_E$ and acts on a node signal $f \in \mathcal{H}_V$ as

$$\nabla_{ij}^{\mathcal{G}} f := f(j) - f(i) \quad (1)$$

for two connected nodes $i, j \in V$. The adjoint of $\nabla^{\mathcal{G}}$ with respect to $\langle \cdot, \cdot \rangle$ as above is given by $\nabla^{\mathcal{G}*} : \mathcal{H}_E \rightarrow \mathcal{H}_V$ acting on $F \in \mathcal{H}_E$ as

$$(\nabla^{\mathcal{G}*} F)(i) = \sum_{e=(j,i)} F(e) - \sum_{e=(i,j)} F(e), \quad (2)$$

where the first sum is over edges oriented toward i and the second over edges oriented away from i .

Proposition 1. For any $f \in \mathcal{H}_V$ and $F \in \mathcal{H}_E$, we have $\langle\langle \nabla^{\mathcal{G}} f, F \rangle\rangle = \langle f, \nabla^{\mathcal{G}*} F \rangle$.

Proposition 2. The positive graph Laplacian induced by the gradient is $L := \text{div}^{\mathcal{G}} \nabla^{\mathcal{G}}$, where the divergence operator is given by $\text{div}^{\mathcal{G}} := -\nabla^{\mathcal{G}*}$. We immediately notice that this is analogous to the Euclidean construction of the Laplace operator $\Delta := \text{div} \nabla$. Moreover, we have

$$L = D - A, \quad (3)$$

where A is the adjacency matrix of \mathcal{G} and D is the degree matrix with entries $D_{ii} = \sum_{j=1}^n A_{ij}$. This matches the well-known definition of the combinatorial graph Laplacian [11].

Eq. (3) is particularly useful, as such an L encodes the connectivity structure of the graph, is symmetric, positive semidefinite, and admits an eigenvalue decomposition of the form $L = U \Lambda U^T$, where $\Lambda = \text{diag}(\lambda_0, \lambda_1, \dots, \lambda_n)$ is the diagonal matrix of ordered eigenvalues $0 \leq \lambda_0 \leq \lambda_1 \leq \dots \leq \lambda_{n-1}$ and U is an orthogonal matrix of eigenvectors.

3.2 Weighted Diffusions Steer & Propagate Information

The diffusion equation models the evolution of a quantity $u : \mathbb{R}^d \times \mathbb{R}_{\geq 0} \rightarrow \mathbb{R}$ that spreads out depending on a diffusion term. Starting from the conservative continuity equation

$$\partial_t u(x, t) = -\nabla \cdot j(x, t), \quad (4)$$

where $j(x, t) = -\mu(x) \nabla u(x, t)$ where $\mu : \mathbb{R}^d \rightarrow \mathbb{R}_+$ is the spatially-dependent diffusivity, we get the following evolution

$$\partial_t u(x, t) = \mu(x) \Delta u(x, t) + \nabla \mu(x) \cdot \nabla u(x, t). \quad (5)$$

When $\mu \equiv 1$, Eq.(5) reduces to $\partial_t u = \Delta u$, with solution $u(t) = e^{t\Delta} u(0)$. When μ varies in space, however, the right-hand side of (5) develops a first-order term in u and therefore has the form of a drift or advection contribution. In this sense, an apparently purely diffusive equation can induce drift-like dynamics once diffusion takes place in an inhomogeneous medium.

This observation is the basis of our approach: instead of prescribing an external drift, we *learn the geometry that induces it*. A positive node-wise weight function μ biases diffusion such that drift-like transport emerges from the operator itself. Learned from data, μ becomes a task-dependent geometric bias that steers information flow through the graph.

3.3 The ChebNet Architecture

The previous section suggests a route to task-adaptive propagation: rather than solving an explicit advection-diffusion PDE or introducing attention-like transport mechanisms, one may seek to encode the transport bias directly into the diffusion operator $\Delta \mapsto \mu\Delta$. On graphs, the natural diffusion operator is the Laplacian L (3). This makes spectral GNNs a natural setting for our construction, since their propagation rules are built directly from L and its spectrum.

ChebNet is particularly well suited to this perspective. It defines graph convolutions through spectral filters of the Laplacian, while avoiding the cost of an explicit eigendecomposition through a polynomial approximation. ChebNet approximates this filter using Chebyshev polynomials, yielding

$$g_\theta(\Lambda) \approx \sum_{k=0}^K \Theta_k T_k(\tilde{\Lambda}), \quad \tilde{\Lambda} = \frac{2\Lambda}{\lambda_{\max}} - I, \quad (6)$$

where T_k is the k -th Chebyshev polynomial and $\tilde{\Lambda}$ rescales the spectrum to the interval $[-1, 1]$. Since polynomials commute with the eigendecomposition, the resulting layer can be written directly in terms of the Laplacian:

$$y = \sum_{k=0}^K T_k(\tilde{L})x\Theta_k, \quad \tilde{L} = \frac{2L}{\lambda_{\max}} - I. \quad (7)$$

This form is crucial: the filter depends only on repeated applications of the Laplacian, and can therefore be evaluated in $O(Km)$ time without computing the eigenvectors explicitly [13].

Consequently, any principled modification of the Laplacian immediately induces a corresponding modification of the propagation geometry, while leaving the spectral architecture essentially unchanged. This makes ChebNet an ideal backbone for our construction: once the learned weight function μ is used to bias the graph Laplacian $L \mapsto L_\mu$, the resulting geometry can be inserted directly into the Chebyshev filtering pipeline.

4 From Weighted Diffusion to a Node-Weighted Graph Laplacian

We now show how to construct biased diffusions on graphs, as done in Section 3.2.

4.1 Weighted Graph Laplacian

Indeed, introducing an external drift term of the form $v(x) \cdot \nabla u(x, t)$, where $v : \mathbb{R}^d \rightarrow \mathbb{R}^d$ is a vector field, into Eq. (5) is not well-defined on graph domains, unlike the continuous setting [14]. Instead, we turn to Dirichlet forms, which admit both \mathbb{R}^d and graph analogs. In finite dimensions, once an inner product $\langle \cdot, \cdot \rangle$ is fixed, a Dirichlet form \mathcal{D} is in one-to-one correspondence [16] with a self-adjoint positive semidefinite Laplacian L through the representation

$$\mathcal{D}(f, g) = \langle f, Lg \rangle, \quad (8)$$

where $f, g \in L^2(\mathbb{R}^d; \mathbb{R})$ in the continuous case, and $f, g \in \mathcal{H}_V$ in the graph case.

Continuous Case. Let $\Omega \subset \mathbb{R}^d$ be a bounded open domain, and let $f, g : \Omega \subset \mathbb{R}^d \rightarrow \mathbb{R}$ be smooth functions vanishing on $\partial\Omega$. For a positive weight function $\mu : \Omega \rightarrow \mathbb{R}_+$, the Dirichlet form given by

$$\begin{aligned} \mathcal{D}_\mu(f, g) &:= \frac{1}{2} \int_\Omega \mu(x) \nabla f(x) \cdot \nabla g(x) dx \\ &= \langle f, \tilde{\Delta}_\mu g \rangle_{L^2(dx)}, \end{aligned} \quad (9)$$

is in one-to-one correspondence to the second-order operator

$$\tilde{\Delta}_\mu f = -\frac{1}{2}\mu\Delta f - \frac{1}{2}\nabla\mu \cdot \nabla f, \quad (10)$$

when considering the usual L^2 inner product. This particular choice of inner product allows us to recover the emerging first-order drift term, previously derived in Eq. (5). We now turn to the case of graphs.

Graph Case. Analogously to the continuous case above, the Dirichlet form on a graph \mathcal{G} with positive node-wise weight function $\mu : V \rightarrow \mathbb{R}_+$ is given by

$$\mathcal{D}_\mu^\mathcal{G}(f, g) = \frac{1}{2} \sum_i \mu_i \sum_{j \sim i} \nabla_{ij}^\mathcal{G} f \nabla_{ij}^\mathcal{G} g, \quad (11)$$

where $\nabla^\mathcal{G}$ is defined as in Eq. (1). In the following result, we derive the corresponding graph operator L_μ in closed form, associated to the edge signal inner product $\langle\langle \cdot, \cdot \rangle\rangle$ from Section 3.

Theorem 1 (Closed form of L_μ). *Let $\mu : V \rightarrow \mathbb{R}_+$ and let $\mathcal{D}_\mu^\mathcal{G}$ be the weighted graph Dirichlet form defined in (11). Then there exists a unique symmetric positive semidefinite matrix L_μ such that $\mathcal{D}_\mu^\mathcal{G}(f, g) = f^\top L_\mu g$. Moreover, L_μ is the weighted graph Laplacian*

$$L_\mu = D_\mu - A_\mu, \quad (12)$$

where $A_\mu = M_\mu \odot A$, $(M_\mu)_{ij} = \frac{\mu_i + \mu_j}{2}$, and $D_\mu = \text{diag}(A_\mu \mathbf{1})$.

Proof. See Appendix C.3. □

Theorem 1 is the weighted analogue of Eq. (3): the standard Laplacian $L = D - A$ is recovered as the special case $A_\mu = A$. The theorem shows that the edge weights are induced by the node-wise weight function μ : each edge (i, j) receives $\frac{1}{2}(\mu_i + \mu_j)$ from its two endpoint values. In particular, the original graph topology is preserved, since $A_{ij} = 0$ implies $(A_\mu)_{ij} = 0$. The weight function therefore changes only the ease of transport along existing edges. The next result makes the analogy with the continuous identity from Eq. (10) explicit.

Theorem 2 (Drift-diffusion decomposition). *Using the graph calculus from Section 3.1, the action of L_μ can be written as*

$$(L_\mu f)_i = \mu_i (L f)_i - \frac{1}{2} \sum_{j \sim i} \nabla_{ij}^\mathcal{G} \mu \nabla_{ij}^\mathcal{G} f, \quad (13)$$

where L is the graph Laplacian as in Eq. (3).

Proof. See Appendix C.4. □

The first term on the right-hand side of Eq. (13) is the usual graph diffusion scaled by the local value μ_i . The second term weights each edge difference of the signal by the corresponding edge difference of μ , so it appears only where the learned density and the signal vary. It is therefore a discrete first-order, drift-like correction induced by the variation of μ . In this sense, it biases diffusion toward selected regions of the graph without introducing an explicit vector field and without modifying the adjacency. See Appendices D and A for details and an additional visualization of the learned density.

4.2 Spectral properties of the L_μ Laplacian

We now show that the weight function μ does more than locally reweight the graph: it reshapes the spectral decay profile of the propagation operator.

Theorem 3 (Spectral comparison). *Let $0 = \lambda_0 \leq \lambda_1 \leq \dots \leq \lambda_{n-1}$ be the eigenvalues of L , and let λ_k^μ denote the eigenvalues of L_μ , ordered similarly. For each $k \in \{0, \dots, n-1\}$, there exist positive constants $c_k^\mu \leq C_k^\mu$, defined in Appendix C.5, such that*

$$\lambda_k \|\mu\|_1 c_k^\mu \leq \lambda_k^\mu \leq \lambda_k \|\mu\|_1 C_k^\mu. \quad (14)$$

The constants c_k^μ and C_k^μ are not universal: they quantify how much μ emphasizes or suppresses the regions where the relevant spectral modes vary. Thus, Theorem 3 should be read as a constrained spectral comparison rather than as free control of individual eigenvalues. Once the scale of μ is fixed, changing μ

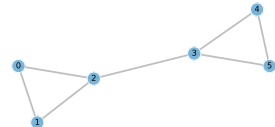


Figure 2: Minimal two-community graph.

does not simply rescale diffusion time. Instead, it redistributes diffusion strength across the graph, changing the relative decay rates of spectral components, experimentally shown in Figure 1 on the SBM.

Avoiding Spectral Redundancy on Bottlenecks Finally, we illustrate the effect of μ on a minimal community graph. Consider two triangles connected by a single bridge edge, the smallest graph with two dense communities and a bottleneck. The standard Laplacian has spectrum $\{0, 0.43, 3, 3, 3, 4.56\}$ where the repeated eigenvalue reflects the graph symmetry: several distinct modes are damped at the same rate under heat diffusion. The first non-zero eigenvector separates the two communities: it is nearly constant within each triangle and changes mainly across the bridge. This makes it the spectral component carrying the community-level information. If we set $\mu = 1.5$ on one community and $\mu = 0.5$ on the other, the weighted Laplacian has spectrum $\{0, 0.38, 1.5, 2.18, 4.5, 5.44\}$. Thus, without changing the edge set, μ breaks the symmetry of the diffusion operator and separates modes that were previously degenerate. The learned density changes the finite-time diffusion regime by making some modes persist longer and others decay faster. We provide a detailed analysis of this phenomenon in Appendix B.

4.3 A novel class of spectral GNNs

The explicit form of the weighted graph Laplacian presented in Theorem 1 matches the form of the combinatorial Laplacian (Eq. (3)) and can therefore be used in any spectral GNN, with minimal modification to the architecture.

Learnable Weight Function. As discussed in Section 4.2, the weight function μ allows control of the spectral properties of L_μ , but it usually remains difficult to design it by hand in practice. We therefore propose a two-step strategy. First, we make a *neural parameterization of μ* . We choose a simple but sufficiently expressive GCN:

$$\mu = \text{GCN}(A, X, \Theta), \tag{15}$$

where A is the adjacency matrix of \mathcal{G} , X is a feature tensor, and Θ consists of learnable weights.

μ -ChebNet Filter. Once μ is learned (15), the second step is to construct L_μ using Eq. (13), and use it directly into a downstream spectral ChebNet. This leads to a new family of architectures, with varying parameterization of μ and downstream ChebNet that can be learned end-to-end to solve a given task. At training time, the weight function μ will be adapted so the downstream μ -ChebNet solves the task and will thus depend on the task and distribution of training samples. As we shall see below, inspecting μ as a graph signal reveals much about the strategy employed by the network.

μ -Stable-ChebNet. A ChebNet variant that is particularly well suited to L_μ is the *Stable-ChebNet* architecture [22], which we also implement in the following experiments.

5 Experiments

We evaluate μ -ChebNet and its stable variant on both synthetic and real-world datasets, to probe various aspects of graph reasoning.

Oversquashing on Barbell Graphs. The *Barbell dataset* [4] synthetically probes oversquashing by requiring nodes in each clique to predict features from the opposite clique, while all cross-clique information must pass through a single bridge edge. Thus, even when the message-passing depth is sufficient for reachability, standard MPNNs must compress many source signals through a narrow graph bottleneck, exposing their inability to transmit long-range information without severe distortion.

Results. We observe in Table 1 that μ -ChebNet significantly outperforms both ChebNet and Stable-ChebNet on barbell graphs of size $N \in \{50, 70\}$. Even in the case of $K = 9$ hops, where Stable-ChebNet struggles, μ -ChebNet achieves almost zero mean square error (MSE). For larger graphs of size $N = 100$, we see in Table 2 that μ -ChebNet lowers the MSE of Stable-ChebNet by an order of magnitude, while having less layers ($K = 15$). Furthermore, we omitted μ -Stable-ChebNet here, as results for μ -ChebNet already demonstrate its improved performance, notably its consistency as graph size increases.

Method	K	50	70
ChebNet	$K = 9$	0.32 ± 0.39	1.08 ± 0.05
	$K = 10$	0.05 ± 0.00	1.08 ± 0.01
Stable-ChebNet	$K = 9$	0.17 ± 0.11	0.47 ± 0.49
	$K = 10$	0.05 ± 0.00	0.06 ± 0.03
μ -ChebNet (ours)	$K = 9$	0.03 ± 0.01	0.02 ± 0.02
	$K = 10$	0.03 ± 0.01	0.02 ± 0.02

Table 1: Mean squared error (MSE) of different ChebNet variants on the oversquashing experiment for barbell graphs of sizes $N = 50, 70$.

Method	K	100
ChebNet	$K = 20$	0.87 ± 0.05
Stable-ChebNet	$K = 20$	0.21 ± 0.27
μ -ChebNet (ours)	$K = 15$	0.02 ± 0.01

Table 2: Mean squared error (MSE) of different ChebNet variants on the oversquashing experiment for barbell graphs of size $N = 100$

Graph Property Prediction. The *Graph Property Prediction* dataset [12] evaluates whether a model can infer global structural quantities of a graph, such as diameter, single-source shortest-path (SSSP) distances, and eccentricity. These tasks test whether a GNN can propagate and integrate information beyond local neighborhoods, exposing limitations in long-range reasoning and structural message diffusion.

Results. We observe in Table 3 that μ -ChebNet systematically improves upon the regular ChebNet formulation, and μ -Stable-ChebNet also improves upon Stable-ChebNet, which itself was demonstrated to strongly outperform existing architectures [22]. We note that while μ -Stable-ChebNet reports a slightly higher mean than Stable-ChebNet for eccentricity, it remains strongly better than all other models, and lies within Stable-ChebNet’s error bars.

Model	Diameter ↓	SSSP ↓	Eccentricity ↓
GCN	0.7424 ± 0.0466	0.9499 ± 0.0001	0.8468 ± 0.0028
GAT	0.8221 ± 0.0752	0.6951 ± 0.1499	0.7909 ± 0.0222
GraphSAGE	0.8645 ± 0.0401	0.2863 ± 0.1843	0.7863 ± 0.0207
GIN	0.6131 ± 0.0990	-0.5408 ± 0.4193	0.9504 ± 0.0007
GCNII	0.5287 ± 0.0570	-1.1329 ± 0.0135	0.7640 ± 0.0355
DGC	0.6028 ± 0.0050	0.1483 ± 0.0231	0.8261 ± 0.0032
GRAND	0.6715 ± 0.0490	-0.0942 ± 0.3897	0.6602 ± 0.1393
A-DGN w/ GCN backbone	0.2271 ± 0.0804	-1.8288 ± 0.0607	0.7177 ± 0.0345
ChebNet	-0.1517 ± 0.0343	-1.8519 ± 0.0539	-1.2151 ± 0.0852
Stable-ChebNet	-0.2477 ± 0.0526	-2.2111 ± 0.0160	-2.1043 ± 0.0766
μ -ChebNet (ours)	-0.2075 ± 0.0634	-2.3149 ± 0.0301	-1.8740 ± 0.0597
+ Stability	-0.3179 ± 0.0182	-2.3217 ± 0.0330	-2.0338 ± 0.0571

Table 3: Mean test set $\log_{10}(\text{MSE})$ and standard deviation averaged over 4 random weight initializations for each configuration on the Graph Property Prediction dataset. The lower the better.

City-Networks Benchmark. We now evaluate our model on the City-Networks dataset [29], a real-world large-scale node classification benchmark derived from city road networks, with graphs built from OpenStreetMap road junctions and segments and labels based on eccentricity/accessibility. The task consists of node classification of city road junctions, requiring information from distant nodes in large-diameter graphs, thereby directly testing real-world long-range reasoning.

Results. We report prediction accuracy (%) results for four different cities (London, Paris, Shanghai, Los Angeles) in Table 4, and observe that μ -ChebNet and its stable variant either outperforms or is within error range of Stable-ChebNet.

Open-Graph Benchmark: Proteins. The ogbn-proteins dataset [23] is a biologically meaningful benchmark, with multi-label protein function prediction tasks on a protein-protein interaction network.

Method	London	Paris	Shanghai	Los Angeles
ChebNet	39.10 ± 1.79	34.34 ± 0.31	40.00 ± 0.39	41.31 ± 0.48
Stable-ChebNet	40.11 ± 0.20	38.11 ± 0.25	41.45 ± 0.27	42.17 ± 0.16
μ-ChebNet (ours)	41.88 ± 0.11	35.14 ± 0.12	41.98 ± 0.96	43.33 ± 0.33
+ Stability	41.44 ± 0.07	37.49 ± 0.26	42.63 ± 0.70	43.10 ± 0.60

Table 4: Accuracy (%) on City-Networks dataset. We use this dataset to fairly compare ChebNet architectures by setting them to the same receptive field $K = 10$ and isolating the effect of the weighted Laplacian L_μ .

Results. We observe in Table 5 that μ -ChebNet reaches a score of 79.36%, outperforming the MPNN baselines [26, 38, 21, 44], and remaining competitive with both Stable-ChebNet [22] and Graph Transformer architectures [6, 39, 41]. Although SPEXFORMER obtains the best score among the reported models, our method achieves comparable performance while relying only on ordinary sparse graph operations. Computationally, μ -ChebNet incurs the cost of a shallow GCN used to learn μ , an $O(m)$ construction of L_μ , and a downstream Chebyshev filter whose propagation cost scales as $O(Km)$, up to feature-channel mixing. Hence, on sparse graphs with fixed K and bounded width, the overall complexity is linear in the number of nodes. By contrast, SPEXFORMER reduces the final attention layer to $O(nd^2 + ndc)$ by selecting c attention edges per node, but requires an additional attention-estimation stage. Thus, while both approaches can scale linearly on sparse graphs, our approach obtains task-adaptive propagation through a learned sparse Laplacian and avoids a two-stage attention-sparsification pipeline.

Discussion and Future Work. Across the experiments, μ -ChebNet is most effective on long-range and bottlenecked tasks, where learning L_μ improves over fixed-Laplacian ChebNet & Stable-ChebNet baselines. On real-world benchmarks, it rivals larger architectures such as graph transformers, while remaining a lightweight end-to-end model. The stability constraint [18, 19, 22] yields mixed gains, improving some benchmarks while leaving others unchanged or slightly worse. This suggests a nontrivial interaction with the learned density μ , whose theoretical and empirical role remains open.

We believe that further important future research lies in deriving tighter eigenvalue bounds for L_μ , evaluating L_μ with other downstream spectral architectures besides ChebNet-style filters, and ablating over alternative parameterizations of μ beyond the GCN considered in this work.

6 Conclusion

In this work, we achieve guided diffusion dynamics on graphs by learning a data-driven weighting μ of the graph nodes, resulting in a task-adaptive graph Laplacian $L_\mu = D_\mu - A_\mu$ (Theorem 1). This produces an end-to-end rewiring-like effect, without changing the graph topology. We prove that this learnable weight function μ allows task-dependent control over the graph’s spectrum by changing the relative decay rates of graph Fourier modes (Theorem 3). Moreover, we introduce μ -ChebNet, an upgraded ChebNet architecture incorporating the modulable graph Laplacian L_μ . We experimentally observe that μ -ChebNet drastically outperforms current ChebNet architectures on signal propagation through narrow bottlenecks (Barbell Graph). On real-world datasets, μ -ChebNet also performs comparably to state-of-the-art architectures. Our work opens doors to further exploring the role of task-adaptive geometry in machine learning, offering better interpretability at a lower cost.

Impact Statement. This work advances the theoretical foundations of graph machine learning by introducing a principled operator that proposes data-driven inhomogeneous diffusion on graphs. While our approach is primarily methodological, future work should consider fairness and bias implications when learning weight functions on graphs.

Model	ROC-AUC \uparrow
MLP	72.04 ± 0.48
GCN	72.51 ± 0.35
ChebNet	77.55 ± 0.43
Stable-ChebNet	79.55 ± 0.34
SGC	70.31 ± 0.23
GCN-NSAMPLER	73.51 ± 1.31
GAT-NSAMPLER	74.63 ± 1.24
SIGN	71.24 ± 0.46
NodeFormer	77.45 ± 1.15
SGFormer	79.53 ± 0.38
SPEXFORMER	80.65 ± 0.07
μ -ChebNet (ours)	79.36 ± 0.41

Table 5: Results on ogbn-proteins.

References

- [1] Adrián Arnaiz-Rodríguez, Ahmed Begga, Francisco Escolano, and Nuria M Oliver. DiffWire: Inductive Graph Rewiring via the Lovász Bound. In Bastian Rieck and Razvan Pascanu, editors, *Proceedings of the First Learning on Graphs Conference*, volume 198 of *Proceedings of Machine Learning Research*, pages 15:1–15:27. PMLR, 09–12 Dec 2022. URL <https://proceedings.mlr.press/v198/arnaiz-rodri-guez22a.html>.
- [2] Álvaro Arroyo, Alessio Gravina, Benjamin Gutteridge, Federico Barbero, Claudio Gallicchio, Xiaowen Dong, Michael Bronstein, and Pierre Vandergheynst. On vanishing gradients, over-smoothing, and over-squashing in gnns: Bridging recurrent and graph learning. *arXiv preprint arXiv:2502.10818*, 2025.
- [3] Hugo Attali, Davide Buscaldi, and Nathalie Pernelle. Rewiring techniques to mitigate over-squashing and over-smoothing in gnns: A survey. *arXiv preprint arXiv:2411.17429*, 2024.
- [4] Jacob Bamberger, Federico Barbero, Xiaowen Dong, and Michael Bronstein. Bundle neural networks for message diffusion on graphs. *arXiv preprint arXiv:2405.15540*, 2024.
- [5] Federico Barbero, Ameya Velingker, Amin Saberi, Michael M. Bronstein, and Francesco Di Giovanni. Locality-aware graph rewiring in GNNs. In *The Twelfth International Conference on Learning Representations*, 2024. URL <https://openreview.net/forum?id=4Ua4hKiAJX>.
- [6] Deyu Bo, Chuan Shi, Lele Wang, and Renjie Liao. Specformer: Spectral graph neural networks meet transformers. *arXiv preprint arXiv:2303.01028*, 2023.
- [7] Joan Bruna, Wojciech Zaremba, Arthur Szlam, and Yann LeCun. Spectral networks and locally connected networks on graphs. *arXiv preprint arXiv:1312.6203*, 2013.
- [8] Benjamin Chamberlain, James Rowbottom, Davide Eynard, Francesco Di Giovanni, Xiaowen Dong, and Michael Bronstein. Beltrami flow and neural diffusion on graphs. *Advances in Neural Information Processing Systems*, 34:1594–1609, 2021.
- [9] Benjamin Paul Chamberlain, James Rowbottom, Maria Gorinova, Stefan Webb, Emanuele Rossi, and Michael M Bronstein. GRAND: Graph neural diffusion. In *International Conference on Machine Learning (ICML)*, pages 1407–1418. PMLR, 2021.
- [10] Jinsong Chen, Kaiyuan Gao, Gaichao Li, and Kun He. Nagphormer: A tokenized graph transformer for node classification in large graphs. *arXiv preprint arXiv:2206.04910*, 2022.
- [11] Fan RK Chung. *Spectral graph theory*, volume 92. American Mathematical Soc., 1997.
- [12] Gabriele Corso, Luca Cavalleri, Dominique Beaini, Pietro Liò, and Petar Veličković. Principal neighbourhood aggregation for graph nets. In *Advances in Neural Information Processing Systems (NeurIPS)*, volume 33, pages 13260–13271, 2020.
- [13] Michaël Defferrard, Xavier Bresson, and Pierre Vandergheynst. Convolutional neural networks on graphs with fast localized spectral filtering. *Advances in neural information processing systems*, 29, 2016.
- [14] Mathieu Desbrun, Anil N Hirani, Melvin Leok, and Jerrold E Marsden. Discrete exterior calculus. *arXiv preprint math/0508341*, 2005.
- [15] Stefano Fiorini, Stefano Coniglio, Michele Ciavotta, and Enza Messina. Sigmanet: One laplacian to rule them all. In *Proceedings of the AAAI Conference on Artificial Intelligence*, volume 37, pages 7568–7576, 2023.
- [16] Masatoshi Fukushima, Yoichi Oshima, and Masayoshi Takeda. *Dirichlet forms and symmetric Markov processes*, volume 19. Walter de Gruyter, 2011.
- [17] Chen Gong, Tongliang Liu, Dacheng Tao, Keren Fu, Enmei Tu, and Jie Yang. Deformed graph laplacian for semisupervised learning. *IEEE transactions on neural networks and learning systems*, 26(10):2261–2274, 2015.

- [18] Alessio Gravina, Davide Bacciu, and Claudio Gallicchio. Anti-Symmetric DGN: a stable architecture for Deep Graph Networks. In *The Eleventh International Conference on Learning Representations*, 2023.
- [19] Alessio Gravina, Moshe Eliasof, Claudio Gallicchio, Davide Bacciu, and Carola-Bibiane Schönlieb. On oversquashing in graph neural networks through the lens of dynamical systems. In *The 39th Annual AAAI Conference on Artificial Intelligence*, 2025.
- [20] Benjamin Gutteridge, Xiaowen Dong, Michael M Bronstein, and Francesco Di Giovanni. Drew: Dynamically rewired message passing with delay. In *International Conference on Machine Learning*, pages 12252–12267. PMLR, 2023.
- [21] Will Hamilton, Zhitao Ying, and Jure Leskovec. Inductive representation learning on large graphs. *Advances in neural information processing systems*, 30, 2017.
- [22] Ali Hariri, Alvaro Arroyo, Alessio Gravina, Moshe Eliasof, Carola-Bibiane Schönlieb, Davide Bacciu, Xiaowen Dong, Kamyar Azizzadenesheli, and Pierre Vandergheynst. Return of chebnet: Understanding and improving an overlooked gnn on long range tasks. *Advances in Neural Information Processing Systems*, 38:136166–136196, 2026.
- [23] Weihua Hu, Matthias Fey, Marinka Zitnik, Yuxiao Dong, Hongyu Ren, Bowen Liu, Michele Catasta, and Jure Leskovec. Open graph benchmark: datasets for machine learning on graphs. In *Proceedings of the 34th International Conference on Neural Information Processing Systems*, NIPS ’20. Curran Associates Inc., 2020. ISBN 9781713829546.
- [24] Yufei Jin and Xingquan Zhu. Oversmoothing alleviation in graph neural networks: a survey and unified view: Y. jin, x. zhu. *Knowledge and Information Systems*, 67(12):11259–11285, 2025.
- [25] Thomas N. Kipf and Max Welling. Semi-Supervised Classification with Graph Convolutional Networks, February 2017. arXiv:1609.02907 [cs].
- [26] TN Kipf. Semi-supervised classification with graph convolutional networks. *arXiv preprint arXiv:1609.02907*, 2016.
- [27] Ron Levie, Wei Huang, Lorenzo Bucci, Michael Bronstein, and Gitta Kutyniok. Transferability of spectral graph convolutional neural networks. *J. Mach. Learn. Res.*, 22(1), January 2021. ISSN 1532-4435.
- [28] Yu Li, Meng Qu, Jian Tang, and Yi Chang. Signed laplacian graph neural networks. In *Proceedings of the AAAI conference on artificial intelligence*, volume 37, pages 4444–4452, 2023.
- [29] Huidong Liang, Haitz Sáez de Ocáriz Borde, Baskaran Sripathmanathan, Michael Bronstein, and Xiaowen Dong. Towards quantifying long-range interactions in graph machine learning: a large graph dataset and a measurement. *arXiv preprint arXiv:2503.09008*, 2025.
- [30] Sohir Maskey, Raffaele Paolino, Aras Bacho, and Gitta Kutyniok. A fractional graph laplacian approach to oversmoothing. *Advances in Neural Information Processing Systems*, 36:13022–13063, 2023.
- [31] Michael Poli, Stefano Massaroli, Junyoung Park, Atsushi Yamashita, Hajime Asama, and Jinkyoo Park. Graph neural ordinary differential equations. *arXiv preprint arXiv:1911.07532*, 2019.
- [32] Ladislav Rampásek, Michael Galkin, Vijay Prakash Dwivedi, Anh Tuan Luu, Guy Wolf, and Dominique Beaini. Recipe for a general, powerful, scalable graph transformer. *Advances in Neural Information Processing Systems*, 35:14501–14515, 2022.
- [33] T. Konstantin Rusch, Michael M. Bronstein, and Siddhartha Mishra. A Survey on Oversmoothing in Graph Neural Networks. *arXiv preprint arXiv:2303.10993*, 2023.
- [34] Franco Scarselli, Marco Gori, Ah Chung Tsoi, Markus Hagenbuchner, and Gabriele Monfardini. The graph neural network model. *IEEE transactions on neural networks*, 20(1):61–80, 2008.

- [35] Zhiqi Shao, Dai Shi, Andi Han, Yi Guo, Qibin Zhao, and Junbin Gao. Unifying over-smoothing and over-squashing in graph neural networks: A physics informed approach and beyond. *arXiv preprint arXiv:2309.02769*, 2023.
- [36] Hamed Shirzad, Ameya Velingker, Balaji Venkatachalam, Danica J Sutherland, and Ali Kemal Sinop. Exphormer: Sparse transformers for graphs. In *International Conference on Machine Learning*, pages 31613–31632. PMLR, 2023.
- [37] Hamed Shirzad, Honghao Lin, Balaji Venkatachalam, Ameya Velingker, David P Woodruff, and Danica J Sutherland. Even sparser graph transformers. *Advances in Neural Information Processing Systems*, 37:71277–71305, 2024.
- [38] Petar Veličković, Guillem Cucurull, Arantxa Casanova, Adriana Romero, Pietro Lio, and Yoshua Bengio. Graph attention networks. In *Proceedings of the International Conference on Learning Representations (ICLR)*, 2018.
- [39] Qitian Wu, Wentao Zhao, Zenan Li, David P Wipf, and Junchi Yan. Nodeformer: A scalable graph structure learning transformer for node classification. *Advances in Neural Information Processing Systems*, 35:27387–27401, 2022.
- [40] Qitian Wu, Chenxiao Yang, Kaipeng Zeng, Fan Nie, Michael Bronstein, and Junchi Yan. Advective diffusion transformers for topological generalization in graph learning. *arXiv preprint arXiv:2310.06417*, 2023.
- [41] Qitian Wu, Wentao Zhao, Chenxiao Yang, Hengrui Zhang, Fan Nie, Haitian Jiang, Yatao Bian, and Junchi Yan. Sgformer: Simplifying and empowering transformers for large-graph representations. *Advances in Neural Information Processing Systems*, 36:64753–64773, 2023.
- [42] Qitian Wu, David Wipf, and Junchi Yan. Transformers from diffusion: A unified framework for neural message passing. *Journal of Machine Learning Research*, 26(129):1–47, 2025.
- [43] Qitian Wu, Chenxiao Yang, Kaipeng Zeng, and Michael M Bronstein. Supercharging graph transformers with advective diffusion. In *Forty-second International Conference on Machine Learning*, 2025.
- [44] Keyulu Xu, Weihua Hu, Jure Leskovec, and Stefanie Jegelka. How powerful are graph neural networks? In *International Conference on Learning Representations (ICLR)*, 2019.
- [45] Xitong Zhang, Yixuan He, Nathan Brugnone, Michael Perlmutter, and Matthew Hirn. Magnet: A neural network for directed graphs. *Advances in neural information processing systems*, 34: 27003–27015, 2021.

A Illustrating enhanced explainability

We provide further evidence that the learned weight function μ helps revealing the strategy used by the network to solve tasks. We consider a dataset of ring graphs and a task that consists in predicting the correct class (among 10) of a query node. This class is encoded as a Dirac in the features of a distant answer node. The query and answer nodes are symmetrically positioned so that there are two long paths of equal lengths connecting them. The features along the first path are all-zero, but the features along the second are i.i.d Gaussian noise. Clearly, agglomerating information along that second path results in accumulating noise and therefore poor decision making. As can be seen on Figure 3, μ assigns higher values to vertices on the most efficient path from the answer node to the query node — effectively steering signal propagation along meaningful routes, without altering the original graph topology. Specifically, μ successfully suppresses one of the two paths, concentrating signal flow along a single route. Beyond improving predictive performance, the learned weight functions offer transparent, interpretable insights into how the model routes information across complex structures.

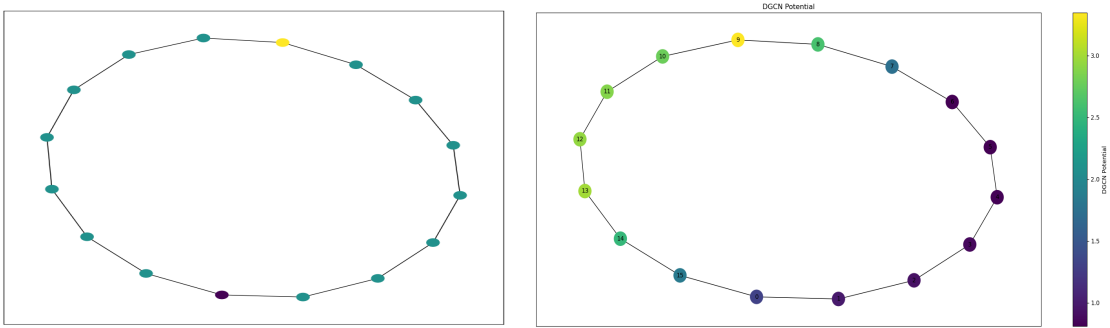


Figure 3: Ring graph configuration. (Left) The query node is in purple and the answer node in yellow. Nodes on the rightward path contain noisy features. (Right) The resulting learned weight function has broken the symmetry of the configuration, routing information on the most informative path.

B Analysis Community Graph

Avoiding Repeated Eigenvalues We consider the graph formed by two triangles connected by a single bridge edge. This graph is a minimal model of a bottlenecked community structure: each triangle is internally dense, while all inter-community communication must pass through one edge. For the standard combinatorial Laplacian, the spectrum is

$$\{0, 0.438, 3, 3, 3, 4.562\}.$$

The repeated eigenvalue at 3 is caused by the symmetry of the two communities. Under heat diffusion, all modes associated with this repeated eigenvalue decay at the same rate. The Fiedler eigenvector, associated with the first non-zero eigenvalue, is aligned with the partition between the two triangles and has a large edge difference on the bridge. We then choose a piecewise constant density μ , with $\mu = 1.5$ on one community and $\mu = 0.5$ on the other, to yield $\sum_i \mu_i = 6 = \sum_{i=1}^6 1$ as for the unweighted case. The spectrum of L_μ becomes

$$\{0, 0.38, 1.5, 2.18, 4.5, 5.44\}.$$

The weighted operator removes the eigenvalue degeneracy and modifies the eigenvectors. Modes whose variations lie mostly in the high- μ region become more costly and are shifted toward larger eigenvalues, while modes varying mostly in the low- μ region remain comparatively slower. Normalizing by the Fiedler eigenvalue gives the relative decay rates

$$L : \{0, 1, 6.84, 6.84, 6.84, 10.40\},$$

whereas

$$L_\mu : \{0, 1, 3.17, 5.70, 15.87, 18.69\}.$$

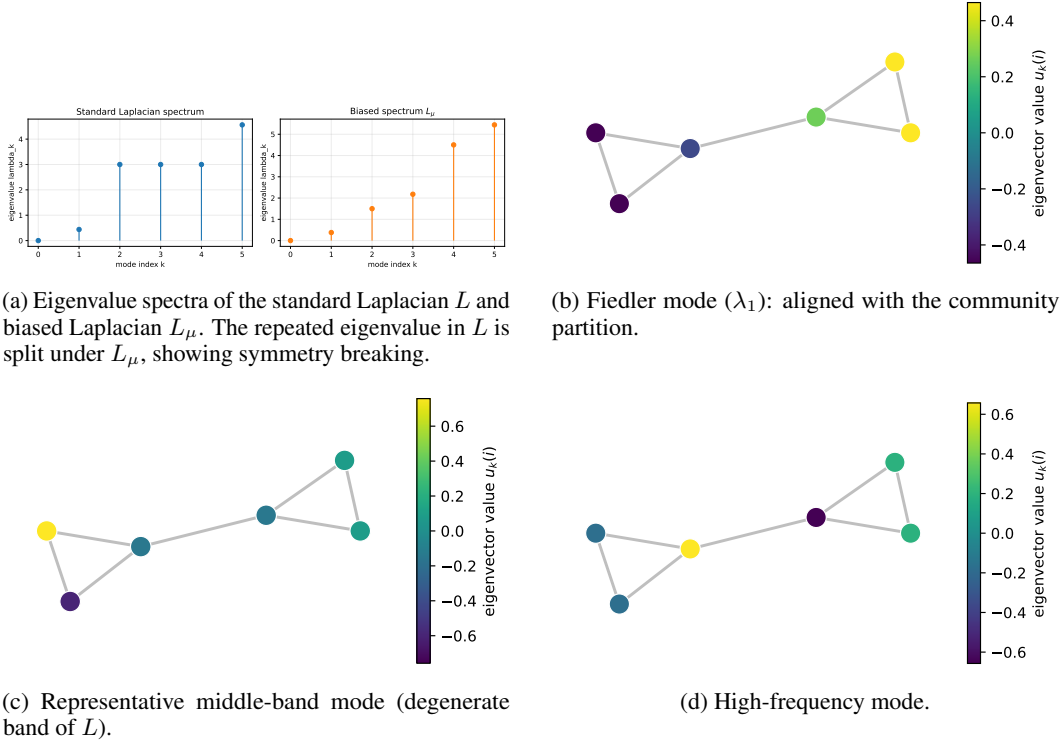


Figure 4: Spectral analysis on the simple community graph.

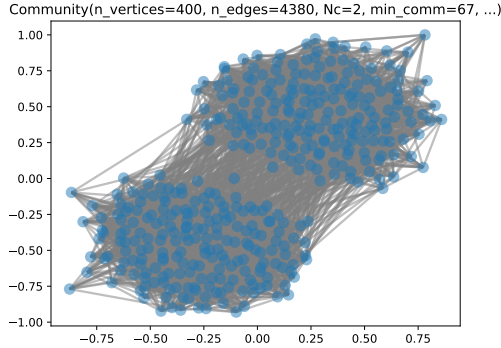


Figure 5: 2-community Graph

This shows that L_μ does not simply accelerate or slow all modes uniformly. Instead, it changes the relative timing of spectral decay: some components become slower relative to the partition mode, while others are damped much faster, as shown in Figure 4. This example highlights the transient nature of the mechanism. Both L and L_μ eventually drive heat diffusion toward the constant eigenspace, so neither operator prevents collapse at infinite time. The difference lies in the finite-time regime relevant for GNNs: L_μ changes which modes remain available before collapse occurs. In this sense, the learned density steers propagation by re-timing spectral decay rather than by inducing faster-than-diffusive transport.

Oversquashing Mitigation via Learned Diffusion Geometry To show how the weighted Laplacian L_μ helps mitigate oversquashing, we perform the following experiment: We generate a 2-community graph C_1 and C_2 with 400 nodes and a strong bottleneck as shown in Figure 5. We choose $\mu = c_1$ on community C_1 and $\mu = c_2$ on community C_2 , where c_1, c_2 are two positive

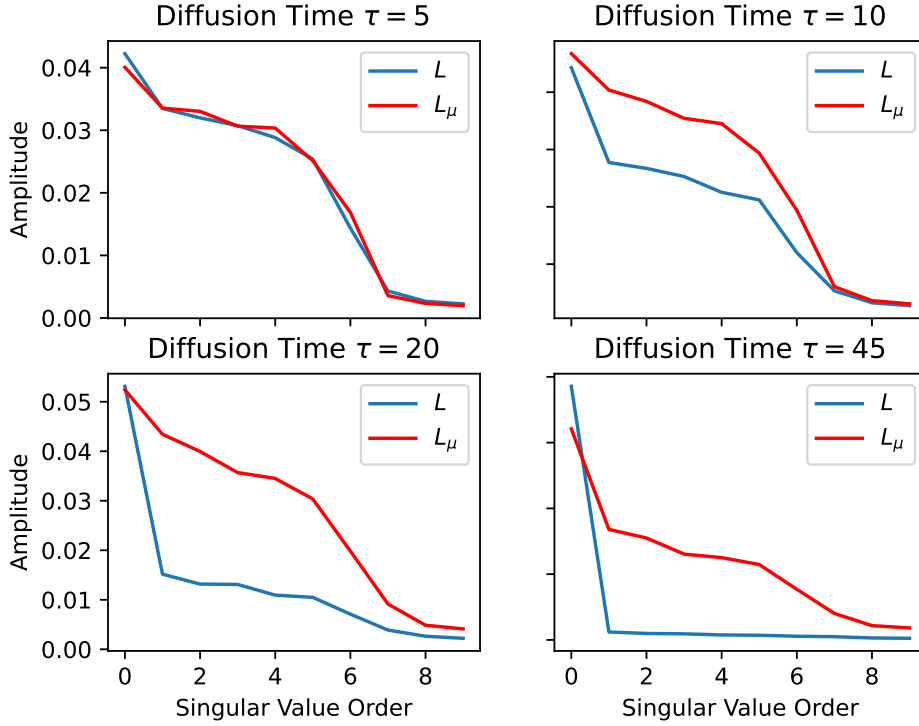


Figure 6: Singular values of the propagated feature matrix restricted to the target cluster. While standard diffusion rapidly collapses all but one direction, the learned weighted diffusion geometry opens a transient regime in which multiple independent directions survive long enough to traverse the bottleneck.

constants. Further, we initiate a feature matrix X_0 consisting of k orthogonal vectors localized on one community. We then propagate using the heat kernels $e^{\tau L}$ and $e^{\tau L_\mu}$ for the weighted Laplacian applied to X_0 . As propagation time τ grows, the signals will transit through the bottleneck to reach the second community. Since the bottleneck is strong, it will limit the flow of information leading to oversquashing. To measure this phenomenon, we track the singular values of the signal restricted to the second community. Under standard diffusion, the effective rank collapses rapidly, indicating severe information compression. In contrast, the weighted Laplacian opens a clear transient regime in which several singular values remain significant, allowing multiple independent directions to traverse the bottleneck before collapse. This demonstrates that the biased diffusion geometry alleviates oversquashing by reallocating spectral mass away from local oscillations and toward bottleneck-aligned transport, as illustrated in Figure 6.

C Proofs

C.1 Proof of Proposition 1

Taking the definitions of ∇^G and ∇^{G^*} from Eqs. (1) and (2), we obtain

$$\langle\langle \nabla^G f, F \rangle\rangle = \sum_{e=(i,j) \in E} (f(j) - f(i))F(e) = \sum_{i \in V} f(i) \left(\sum_{e=(j,i)} F(e) - \sum_{e=(i,j)} F(e) \right) = \langle f, \nabla^{G^*} F \rangle. \quad (16)$$

proving the claim. \square

C.2 Proof of Proposition 2

For any node i ,

$$(\nabla^{\mathcal{G}^*} \nabla^{\mathcal{G}} f)(i) = \sum_{e=(j,i)} (\nabla^{\mathcal{G}} f)(e) - \sum_{e=(i,j)} (\nabla^{\mathcal{G}} f)(e).$$

If $e = (j, i)$, then $(\nabla^{\mathcal{G}} f)(e) = f(i) - f(j)$. If $e = (i, j)$, then $(\nabla^{\mathcal{G}} f)(e) = f(j) - f(i)$, so the second term contributes $f(i) - f(j)$. Hence

$$(\nabla^{\mathcal{G}^*} \nabla^{\mathcal{G}} f)(i) = \sum_{j \sim i} (f(i) - f(j)) = (D - A)f(i).$$

Therefore $\nabla^{\mathcal{G}^*} \nabla^{\mathcal{G}} = D - A$. The divergence identity follows from $\text{div}^{\mathcal{G}} := -\nabla^{\mathcal{G}^*}$.

□

C.3 Proof of Theorem 1

We first consider a non-negative node-wise weight $\mu : V \rightarrow \mathbb{R}^+$ and the corresponding Dirichlet bilinear form: $\mathcal{D}_\mu^{\mathcal{G}}(f, g) = \frac{1}{2} \sum_i \mu_i \sum_{j \sim i} \nabla_{ij}^{\mathcal{G}} f \nabla_{ij}^{\mathcal{G}} g$.

Developing $\mathcal{D}_\mu^{\mathcal{G}}$ we get:

$$\begin{aligned} \mathcal{D}_\mu^{\mathcal{G}}(f, g) &= \frac{1}{2} \sum_i \mu_i \sum_{j \sim i} \nabla_{ij}^{\mathcal{G}} f \nabla_{ij}^{\mathcal{G}} g \\ &= \frac{1}{2} \sum_i \mu_i \sum_{j \sim i} (g(i) - g(j))(f(i) - f(j)) \\ &= \frac{1}{2} \sum_i \sum_{j \sim i} \frac{\mu_i S_{ij} + \mu_j S_{ji}}{2} \\ &= \frac{1}{2} \sum_i \sum_{j \sim i} \frac{S_{ij}(\mu_i + \mu_j)}{2} \\ &= \sum_{i \sim j} \frac{\mu_i + \mu_j}{2} (f(i) - f(j))(g(i) - g(j)) \\ &= \frac{1}{2} \sum_i \sum_j A_{\mu, ij} (f(i) - f(j))(g(i) - g(j)) \\ &= \frac{1}{2} \sum_i \sum_j g(i) A_{\mu, ij} (f(i) - f(j)) - g(j) A_{\mu, ij} (f(i) - f(j)) \\ &= \frac{1}{2} \sum_i \sum_j g(i) A_{\mu, ij} (f(i) - f(j)) - g(i) A_{\mu, ji} (f(j) - f(i)) \\ &= \sum_i \sum_j g(i) A_{\mu, ij} (f(i) - f(j)) \\ &= \sum_i g(i) \left(D_{\mu, ii} f(i) - \sum_{j \sim i} A_{\mu, ij} f(j) \right) \end{aligned}$$

where we have defined $A_\mu = M_\mu \odot A$, with \odot being the Hadamard product and $M_{\mu, ij} = \frac{1}{2}(\mu_i + \mu_j)$. On line 3, we have defined $S_{ij} = (f(i) - f(j))(g(i) - g(j))$. On line 4, we use the symmetry property of the matrix S . A similar reasoning has been used on line 8, since $A_{\mu, ij}$ is also symmetric. The weighted adjacency matrix A_μ preserves the original adjacency and the corresponding degree matrix is defined as usual $D_\mu = \text{diag}(A_\mu \mathbf{1})$. Finally, we immediately see that:

$$D_\mu^{\mathcal{G}}(f, g) = (L_\mu f)^T g \Rightarrow L_\mu = D_\mu - A_\mu \quad (17)$$

Which allows us to just simply compute A_μ and D_μ .

□

C.4 Proof of Theorem 2

We derive the decomposition of L_μ :

$$\begin{aligned}
(L_\mu f)_i &= \sum_{j \sim i} \frac{\mu_i + \mu_j}{2} (f(i) - f(j)) \\
&= \sum_{j \sim i} \left(\mu_i + \frac{\mu_j - \mu_i}{2} \right) (f(i) - f(j)) \\
&= \mu_i \sum_{j \sim i} (f(i) - f(j)) + \frac{1}{2} \sum_{j \sim i} (\mu_j - \mu_i) (f(i) - f(j)) \\
&= \mu_i (L f)(i) - \frac{1}{2} \sum_{j \sim i} \nabla_{ij}^G \mu \nabla_{ij}^G f.
\end{aligned}$$

□

C.5 Proof of Theorem 3

Since L_μ preserves the graph topology, its effect comes from changing the contribution of local differences $f(u) - f(v)$ (where u and v are two neighboring nodes) to the Dirichlet energy. This section makes this precise through Rayleigh quotients, derives bounds comparing the spectra of L and L_μ , and illustrates how μ can modulate the spectral gap, the spectral radius, and repeated eigenvalues.

First, we compare L and L_μ through their Rayleigh quotients, $\mathcal{R}(f) = \frac{f^\top L f}{f^\top f}$, and $\mathcal{R}_\mu(f) = \frac{f^\top L_\mu f}{f^\top f}$. For $f \in \mathbb{R}^n$, define the normalized local variation profile

$$N(f) = \left(\frac{\|\nabla^G f(u)\|_2^2}{f^\top f} \right)_{u \in V}, \text{ where } \|\nabla^G f(u)\|_2^2 = \sum_{v \sim u} (f(u) - f(v))^2, \text{ and the associated probability distribution } p_f = \frac{1}{\mathbf{1}^\top N(f)} N(f).$$

In order to complete the proof, let us first state a helpful lemma:

Lemma C.1 (Rayleigh quotient factorization). *Let $f \in \mathbb{R}^n$. Then*

$$\mathcal{R}_\mu(f) = \|\mu\|_1 \mathbb{E}_\mu[p_f] \mathcal{R}(f),$$

where $\mathbb{E}_\mu[p_f]$ is the expectation of p_f under μ normalized to be a probability distribution.

Lemma C.1 shows that μ controls the spectrum by changing the cost of local variations: if μ is large where f varies strongly, then $\mathcal{R}_\mu(f)$ increases; if μ is small in those regions, it decreases. The spectrum of L_μ is therefore controlled by the global scale $\|\mu\|_1$, the spectrum of the underlying graph through $\mathcal{R}(f)$, and the alignment between μ and the local variation profile p_f .

Theorem 3 shows that shaping μ gives targeted control over the spectrum, beyond a global rescaling by $\|\mu\|_1$. In particular, eigenvalues can be increased or decreased depending on how the potential overlaps with the local variation profiles of the corresponding eigenvectors. In the next section, we therefore parameterize μ and use the resulting Laplacian as an adaptive propagation operator in spectral GNN architectures.

We only prove the upper bound as the same reasoning applies to the lower bound. Let's define the set of Euclidian subspaces of \mathbb{R}^n ,

$$\mathcal{F}_k = \{F, \dim(F) = k + 1 \text{ and } \lambda_k = \max \{ \mathcal{R}(f) \mid f \in F, \|f\|_2 = 1 \} \}$$

and fix $F \in \mathcal{F}_k$. By Lemma C.1

$$\begin{aligned}
\max_{\substack{f \in F \\ \|f\|_2=1}} \mathcal{R}_\mu(f) &= \max_{\substack{f \in F \\ \|f\|_2=1}} \|\mu\|_1 \mathbb{E}_\mu[p_f] \mathcal{R}(f) \\
&\leq \|\mu\|_1 \left(\max_{\substack{f \in F \\ \|f\|_2=1}} \mathbb{E}_\mu[p_f] \right) \left(\max_{\substack{f \in F \\ \|f\|_2=1}} \mathcal{R}(f) \right) = \lambda_k \|\mu\|_1 \max_{\substack{f \in F \\ \|f\|_2=1}} \mathbb{E}_\mu[p_f].
\end{aligned}$$

Thus

$$\min_{F \in \mathcal{F}_k} \max_{\substack{f \in F \\ \|f\|_2=1}} \mathcal{R}_\mu(f) \leq \lambda_k \|\mu\|_1 \min_{F \in \mathcal{F}_k} \max_{\substack{f \in F \\ \|f\|_2=1}} \mathbb{E}_\mu[p_f].$$

And

$$\min_{\substack{F \subset \mathbb{R}^n \\ \dim(F)=k+1}} \max_{\substack{f \in F \\ \|f\|_2=1}} \mathcal{R}_\mu(f) \leq \min_{F \in \mathcal{F}_{k+1}} \max_{\substack{f \in F \\ \|f\|_2=1}} \mathcal{R}_\mu(f),$$

where

$$\min_{\substack{F \subset \mathbb{R}^n \\ \dim(F)=k+1}} \max_{\substack{f \in F \\ \|f\|_2=1}} \mathcal{R}_\mu(f) = \lambda_k^\mu$$

by the min-max theorem. □

C.6 Proof of Lemma C.1

We simply write:

$$\mathcal{R}_\mu(f) = \frac{1}{2} \mu^\top \cdot N(f) = \|\mu\|_1 \left(\frac{1}{\|\mu\|_1} \mu^\top \cdot p_f \right) \cdot \frac{1}{2} (\mathbf{1}^\top \cdot N(f)) = \|\mu\|_1 \mathbb{E}_\mu[p_f] \mathcal{R}(f). \quad \square$$

D Details on Section 4.1

We now introduce the geometric construction underlying our approach. Rather than adding an explicit advection field to a diffusion equation, we modify the diffusion geometry itself through a positive weight μ . This distinction is important on graphs. In the continuous setting, a term such as $v \cdot \nabla f$ for a scalar function f and v a vector field, is well defined because both $v(x)$ and $\nabla f(x)$ live in the same tangent space. On a graph, however, node signals live on vertices, whereas discrete gradients naturally live on edges. Defining a vector field therefore requires additional non-canonical choices, such as an orientation. Dirichlet forms and Laplacians, in contrast, admit direct graph analogues. This motivates inducing a transport bias through a weighted diffusion geometry rather than by prescribing an explicit advective field.

We first recall the unweighted continuous case. Let $f, g : \Omega \subset \mathbb{R}^d \rightarrow \mathbb{R}$ be smooth functions vanishing on $\partial\Omega$. The standard Dirichlet form is $\mathcal{D}(f, g) = \frac{1}{2} \int_\Omega \nabla f(x) \cdot \nabla g(x) dx$. By integration by parts, using the boundary condition, one obtains $\mathcal{D}(f, g) = -\frac{1}{2} \int_\Omega g(x) \Delta f(x) dx$. Hence, with respect to the standard $L^2(dx)$ inner product, the associated positive operator is $Lf = -\frac{1}{2} \Delta f$. The corresponding gradient flow is the usual heat equation $\partial_t f = -Lf = \frac{1}{2} \Delta f$. Thus, the standard Dirichlet form recovers the usual Laplacian and ordinary diffusion. We now introduce a positive weight $\mu : \Omega \rightarrow \mathbb{R}_{>0}$ and define the weighted Dirichlet form $\mathcal{D}_\mu(f, g) = \frac{1}{2} \int_\Omega \mu(x) \nabla f(x) \cdot \nabla g(x) dx$. This form penalizes local variations differently depending on the position. Equivalently, μ changes the geometry in which diffusion takes place.

There are two useful ways of representing the operator associated with the same Dirichlet form. First, using the weighted inner product $\langle f, g \rangle_\mu = \int_\Omega f(x) g(x) \mu(x) dx$, integration by parts gives $\mathcal{D}_\mu(f, g) = \langle g, L_\mu f \rangle_\mu$, where

$$L_\mu f = -\frac{1}{2\mu} \nabla \cdot (\mu \nabla f) = -\frac{1}{2} \Delta f - \frac{1}{2} \nabla \log \mu \cdot \nabla f. \quad (18)$$

The second term in (18) is first order and therefore has the form of a drift or advective contribution. However, it is not introduced through an independently prescribed velocity field. It is induced by the spatial variation of the weight μ .

Equivalently, one may represent the same Dirichlet form using the standard $L^2(dx)$ inner product. This gives

$$\tilde{L}_\mu f = -\frac{1}{2} \nabla \cdot (\mu \nabla f) = -\frac{1}{2} \mu \Delta f - \frac{1}{2} \nabla \mu \cdot \nabla f. \quad (19)$$

The associated diffusion equation is $\partial_t f = -\tilde{L}_\mu f$. This second representation gives the intuition of a diffusion with spatially varying diffusivity μ . Expanding the weighted diffusion operator in (19) produces the first-order term $\nabla \mu \cdot \nabla f$, which acts as a drift-like bias. It appears because the diffusion weight itself varies in space. This is the continuous mechanism that we now transfer to graphs.

In the unweighted graph case, the Dirichlet form is $\mathcal{D}^G(f, g) = \frac{1}{2} \sum_{i,j} A_{ij} (f_i - f_j)(g_i - g_j)$. Using the symmetry of A , this rewrites as $\mathcal{D}^G(f, g) = \sum_i g_i \sum_j A_{ij} (f_i - f_j) = g^\top (D - A)f$. Thus, as in the continuous case, the operator represented by the unweighted graph Dirichlet form is the combinatorial Laplacian $L = D - A$.

E Experimental setup

E.1 Hyper-parameters

We report in Tables 6 and 7 the hyper-parameters used in Section 5.

Hyper-parameter	Values in grid	Diam	SSSP	Ecc
Hidden dimension d	20, 30, 50	50	30	30
Number of layers	1, 2, 3, 5, 10, 20	20	5	5
Polynomial order K	3, 5, 10	4	10	10
Step size ϵ	0.01, 0.10, 0.20, 0.30	0.40	0.30	0.30
Dissipative force γ	0, 0.01, 0.50, 1	0.01	0.00	0.00
Activation function	tanh, relu	relu	relu	relu
Learning rate	0.001, 0.003	0.003	0.003	0.003
Weight decay	1×10^{-6}	1×10^{-6}	1×10^{-6}	1×10^{-6}

Table 6: Hyper-parameter grid and best settings for our model on three synthetic graph-property benchmarks.

Hyper-parameter	Sweep
Hidden dim d	256, 512, 1024
Polynomial order K	5, 10, 15
Num of layers	3, 5, 7
MLP layers	1, 2, 3
Step size ϵ	[0.1, 1.0]
Dissipative force γ	0.01, 0.05, 0.1
Batch size	512, 1024, 2048
Learning rate	0.0005, 0.001, 0.005
Optimizer	Adam
Pos-enc type	None, Laplacian, RW
Pos-enc dim	16, 32, 64

Table 7: Hyper-parameter sweep ranges for our model on ogbn-proteins.

E.2 Barbell task description

The Barbell dataset is designed to test whether a GNN can transmit information across a severe graph bottleneck. Each graph consists of two densely connected complete subgraphs, called the “bells,” joined by a narrow path or “bridge” as shown in Figure 7. Nodes inside each bell are highly connected, while the bridge is the only route through which information can pass from one side of the graph to the other. The learning task is node-level regression: each node must predict the average input feature of the nodes in the opposite bell. This makes the dataset a direct probe of long-range communication, because successful prediction requires information to cross the bridge rather than remain trapped within one dense cluster. Performance is measured using mean squared error (MSE), where high

errors indicate either over-squashing, when information from the opposite bell fails to pass through the bridge, or over-smoothing, when node representations collapse and lose local distinctions.

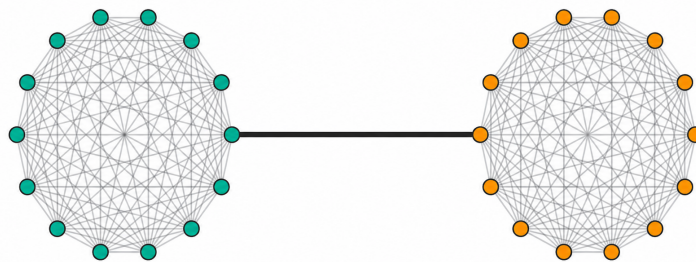


Figure 7: Illustration of a Barbell graph composed of two densely connected node clusters